DOI: 10.1007/s11099-018-0779-7 PHOTOSYNTHETICA 56 (1): 265-274, 2018

The phycobilisome terminal emitter transfers its energy with a rate of (20 ps)$^{-1}$ to photosystem II

A.M. ACUÑA[*], P. VAN ALPHEN[**], R. VAN GRONDELLE[*], and I.H.M. VAN STOKKUM[*,+]

Institute for Lasers, Life and Biophotonics, Faculty of Sciences, Vrije Universiteit Amsterdam, De Boelelaan 1081, 1081 HV, Amsterdam, The Netherlands[*]
Swammerdam Institute for Life Sciences, University of Amsterdam, 1098 XH, Amsterdam, The Netherlands[**]

Abstract

Ultrafast time resolved emission spectra were measured in whole cells of a PSI-deficient mutant of *Synechocystis* sp. PCC 6803 at room temperature and at 77K to study excitation energy transfer and trapping. By means of a target analysis it was estimated that the terminal emitter of the phycobilisome, termed allophycocyanin 680, transfers its energy with a rate of (20 ps)$^{-1}$ to PSII. This is faster than the intraphycobilisome energy transfer rates between a rod and a core cylinder, or between the core cylinders.

Additional key words: excitation energy transfer; global analysis; light harvesting; target analysis.

Introduction

Photosynthesis is key to the conversion of solar energy to biomass. Light-harvesting antennae absorb sunlight and transfer the excitation energy ultimately to the reaction centers (RCs) (Mirkovic *et al.* 2017). The phycobilisome (PB) is the light-harvesting antenna of many cyanobacteria, red algae, and glaucophytes (Glazer 1984, Adir 2005, Watanabe and Ikeuchi 2013). Light is absorbed by phycocyanobilin pigments that are covalently bound to phycobiliproteins (Glazer 1984). The rods and core contain phycocyanin (PC) and allophycocyanin (APC), respectively. Together these pigments absorb light between 400 and 650 nm, and excitations of the antenna pigments are efficiently transferred to the chlorophyll-containing PSI and PSII (Gillbro *et al.* 1985, Sandström *et al.* 1988, Tian *et al.* 2011, 2012, 2013b; Scott *et al.* 2006, Liu *et al.* 2013). These photosystems convert the excitations to chemical energy *via* initial charge separation (van Grondelle *et al.* 1994), and the combined action of PBs and photosystems (the light reactions of photosynthesis) provides the energy input to the cell (Govindjee *et al.* 2017). Until now, the rate at which the phycobilisome transfers its energy to PSII is not known. Here we measure ultrafast time resolved emission spectra in whole cells of a PSI-deficient mutant of the cyanobacterium *Synechocystis* sp. PCC 6803 (Shen *et al.* 1993). With the help of target analysis (Holzwarth 1996, van Stokkum *et al.* 2004) we estimated the unknown rate of energy transfer from PB to PSII.

Fig. 1 schematically depicts the fluorescent species that we expect to be present, and the excitation energy transfer (EET) pathways from the PB rods *via* the core cylinders to the PSII dimer. Next to the PB-PSII complex with both PSII RCs open (Fig. 1*A*), part of the complexes may have both PSII RCs closed (Fig. 1*B*). Additionally, over the time course of an experiment (typically 50–90 min) the sample may change, and part of the PB may no longer be coupled to any PSII (Fig. 1*C*). Finally, a small fraction of uncoupled PSII dimers with open (Fig. 1*D*) or closed

Received 14 June, *accepted* 25 August 2017, *published as online-first* 10 January 2018.
[+]Corresponding author; e-mail: ivo@few.vu.nl
Abbreviations: APC – allophycocyanin; DAS – decay-associated spectrum; ΔPSI – PSI-deficient mutant of *Synechocystis* sp. PCC 6803; EAS – evolution-associated spectrum; ET – electron transfer; EET – excitation energy transfer; FWHM – full width at half maximum; IRF – instrument response function; PB – phycobilisome; PC – phycocyanin; rms – root mean square; RP – radical pair; SAS – species-associated spectrum; SNR – signal to noise ratio; SS – steady-state spectra; SVD – singular value decomposition; TRES – time resolved emission spectrum; WT – wild type.
Acknowledgments: The ΔPSI mutant which was originally constructed by Wim Vermaas (Arizona State University, Tempe, Arizona, USA) was kindly provided to us by Christiane Funk (Umeå University, Sweden). This research was performed as part of the BioSolar Cells research program, sponsored by the Dutch Ministry of Economic Affairs. This work is part of the research program of the Netherlands Organization for Scientific Research (NWO, previously FOM). IHMvS and RvG acknowledge financial support of the European Research Council [Advanced Grant proposal 267333 (PHOTPROT) to RvG].

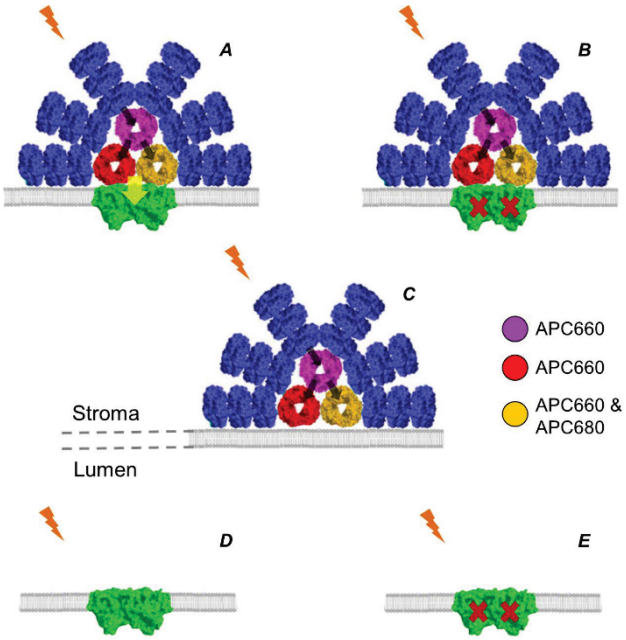

Fig. 1. Cartoon of possible fluorescent species in the *Synechocystis* ΔPSI mutant. Depicted are a PB-PSII complex with both PSII RCs open (*A*), both closed (*B*), a PB that is not coupled to any PSII (*C*) as well as an uncoupled PSII dimer with open (*D*) and closed (*E*) RCs. *Key:* blue, rods consisting of three hexamers; top and basal core cylinders respectively in magenta, red and orange; green, PSII dimer. Dark arrows represent intra-PB EET; yellow arrows represent EET from the PB core to PSII. An "X" stands for a closed PSII RC.

(Fig. 1*E*) RCs may be present.

Fig. 2 depicts the different pigments present in a PB-PSII complex. Recently, a functional compartmental model of the PB has been developed (van Stokkum *et al.* 2017). A compartment contains pigments with the same light-harvesting function that are considered equivalent. The four colors that are used in Fig. 2 for the core; magenta, red, orange, and black indicate the four groups of pigments that will be lumped into four compartments. Below, the rods will be described by two compartments (PC640 and PC650). The PSII RC contains 6 Chl *a* and 2 Pheo, the core antennae CP43 and CP47 contain 14 and 17 Chl *a,* respectively. At room temperature (RT), the 37 Chl *a* and the 2 Pheo will be lumped in one Chl *a* compartment. In Fig. 2, a green barrel symbolizes the PSII core containing 39 chlorins. The biexponential decay of the PSII dimer emission (Tian *et al.* 2013a) will be described by an equilibrium of the Chl *a* compartment with a radical pair (RP) compartment. Thus we will arrive at a minimal model of twelve compartments (cf. Fig. 4*E*). Microscopic rate constants describe the rates of EET/ET between the compartments. The spectral properties of the different compartments will be described by species associated spectra (SAS). The parameters of this target model will be estimated from the time resolved emission spectra. Below we will first globally analyze the RT emission data and based thereupon develop a functional compartmental model for the PB-PSII complex. Then, we will verify whether this model also holds at 77K.

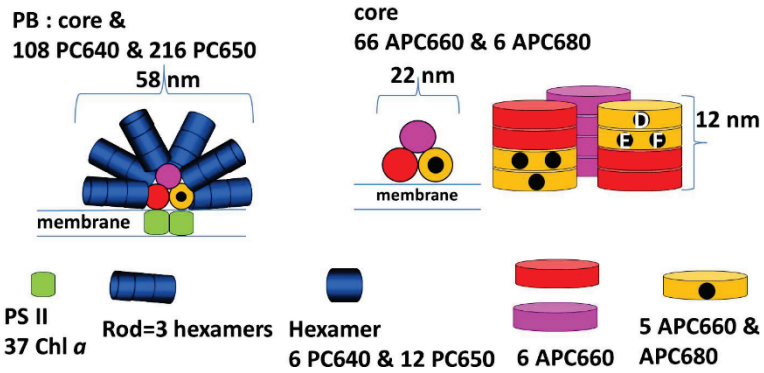

Fig. 2. The structure of PB-PSII is shown schematically, and the most important pigments are indicated. Each rod contains three hexamers. PC rods in blue (total number of PC640 and PC650 pigments indicated). APC that fluoresces at 660 nm (APC660) in magenta, red and orange (66 pigments in total), and the low-energy part of APC indicated by black dots (six APC680 pigments in total). The letters *D,E,F* indicate the three different APC680 pigments. The approximate length for each subunit is based on (Arteni *et al.* 2009).

Materials and methods

Growth conditions and sample preparation: The PSI-deficient mutant of *Synechocystis* (Shen *et al.* 1993) was a gift from prof. C. Funk (Umeå University, Sweden) and was stored at –80°C in 15% glycerol. Prior to preparing a liquid culture, cells were streaked on agar plates containing *BG-11* (*Sigma*) supplemented with 0.3% sodium thiosulfate, 35 μg(chloramphenicol) mL^{-1}, and 10 mM glucose. The strain appeared incompatible with our usual agar, requiring the plates to be solidified using *Difco* granulated agar (*BD*). The plates were incubated in an incubator (*Versatile Environmental Test Chamber MLR-350H*, *Sanyo*, Japan) with a humidified atmosphere of elevated CO_2 (2%) kept at 30°C. Incident light intensity was reduced to below 5 μmol(photon) m^{-2} s^{-1} by covering

the plates with layers of paper.

Liquid cultures were prepared by inoculating 25 mL of modified *BG-11* (*BG-11-PC*, van Alphen *et al.* manuscript in preparation) supplemented with 10 mM glucose, 25 mM 1,4-piperazinedipropanesulfonic acid (PIPPS)–KOH buffered at pH 8.0 and 5 μg(chloramphenicol) mL^{-1} in a 100-mL flask (*FB33131*, *Fisherbrand*). The flasks were covered in multiple layers of paper to reduce the incident light intensity to below 5 μmol(photon) m^{-2} s^{-1} and were placed in a shaking incubator (*Innova 43*, *New Brunswick Scientific*), equipped with a custom built LED panel containing LEDs of 632 nm (orange-red) and 451 nm (blue, both 8 nm full width at half maximum) at 120 rpm and 30°C.

Steady-state absorption of whole cells was measured using a *Varian Cary 4000* UV-Vis spectrophotometer additionally equipped with a *Varian 900* external diffuse reflectance accessory.

Time-resolved fluorescence: A series of streak camera measurements (van Stokkum *et al.* 2008, Wlodarczyk *et al.* 2016), comprising several image sequences using different parameters, was carried out less than one hour after taking the cells out of the reactor to ensure excellent sample quality. While there is no evidence for significant cell degradation during single sequences, the cells may have changed from one sequence to the next. The different conditions from one sequence to another include two different excitation wavelengths (400 nm for predominant Chl excitation; 590 nm for predominant PB excitation), or different time ranges (TR): from 0 to 400 ps (TR2) and from 0 to 1500 ps (TR4). For measurements performed using TR2 (TR4), the image sequence consists of 300 (150) images, each of which results from a scan of 8 s. In order to achieve a high SNR, each image sequence is used to produce an average image that is, in its turn, corrected for background and lamp shading before analysis. In order to judge whether the sample changed over time, we kept track of the chronological order in sequence acquisition. We indicate the conditions as 'time range/λ_{exc} (in nm)'. Measurements were done at room temperature (RT) and at 77K. The acquisition order at RT was: TR2/590 → TR4/590 → TR4/400 → TR2/400. The acquisition order at 77K was: TR2/400 → TR4/400 → TR4/590 → TR2/590.

The samples frozen to 77K in a Pasteur pipette were placed in a cold finger. The diameter of the excitation beam and the optical path length within the sample were both ≈1 mm. The fluorescence at the angle of 90° to the direction of the excitation beam was collimated and focused onto the input slit of spectrograph *Chromex 250IS* (*Chromex*, Albuquerque, New Mexico). In one case (77K, 590 nm exc) a cut off filter *OC14* was used to block the scattered excitation light. The spectrally resolved emission was detected using a *Hamamatsu C5680* synchroscan camera with a cooled *Hamamatsu* digital camera *C10600-10B* (*ORCA-R2*) (*Hamamatsu Photonics*, Hamamatsu, Japan). In all cases, the laser light was vertically polarized, the laser power was 15 μW, the spot size was of 60 μm, the laser repetition rate was set to 250 kHz, the input slit of the spectrograph was 140 μm and that of the photo-cathode of the streak camera was 220 μm and the detection was parallel (VV) to the incident polarization. At RT, the full width at half maximum (FWHM) of the instrument αresponse function (IRF) was ≈7 ps with TR2 and ≈18 ps with TR4. At 77K, The FWHM of the IRF was ≈13 ps with TR2 and ≈25 ps with TR4.

Global and target analysis of time resolved emission spectra: In target analysis of time resolved emission spectra, the inverse problem is to determine the number of electronically excited states (N_{states}) present in the system, and to estimate their spectral properties $SAS_l(\lambda)$ (and their populations $c_l^S(t)$ (superscript S stands for species). The time resolved emission spectra TRES(t,λ) are described by a parameterized superposition model:

$$\mathrm{TRES}(t,\lambda) = \sum_{l=1}^{\mathrm{Nstates}} c_l^S(t,\theta)\mathrm{SAS}_l(\lambda)$$

where the populations are determined by an unknown compartmental model, that depends upon the unknown kinetic parameters θ. In the target analysis constraints on the SAS are needed to estimate all parameters θ and $SAS_l(\lambda)$ (van Stokkum *et al.* 2004, Snellenburg *et al.* 2013).

The population of the *l*-th compartment is $c_l^S(t)$. The concentrations of all compartments are collated in a vector:

$$c^s(t) = \left[c_1^S(t)c_2^S(t) \ldots c_{n_{comp}}^S(t)\right]$$

which obeys the differential equation

$$\frac{d}{dt}c^S(t) = Kc^S(t) + j(t)$$

where the transfer matrix *K* contains off-diagonal elements k_{pq}, representing the microscopic rate constant for energy transfer from compartment *q* to compartment *p*. The diagonal elements contain the total decay rates of each compartment. The input to the compartments is $j(t) = \mathrm{IRF}(t)\left[x_1 \ldots x_{n_{comp}}\right]$, with x_l the absorption of the *l*-th compartment.

The impulse response of the system, which is a sum of exponential decays, has to be convolved with the IRF. Typically, a Gaussian shaped IRF is adequate, with parameters μ for the location of the IRF maximum and Δ for the FWHM of the IRF:

$$\mathrm{IRF}(t) = \frac{1}{\widetilde{\Delta}\sqrt{2\pi}}\exp\left(-\log(2)\left(\frac{2(t-\mu)}{\Delta}\right)^2\right)$$

where $\widetilde{\Delta} = \Delta/\left(2\sqrt{2\log(2)}\right)$. The convolution (indicated by an *) of this IRF with an exponential decay (with decay rate *k*) yields an analytical expression which facilitates the estimation of the decay rate *k* and the IRF parameters μ and Δ:

$$c^D(t,k,\mu,\Delta) = \exp(-kt) * IRF(t) = \frac{1}{2}\exp(-kt)\exp\left(k\left(\mu + \frac{k\tilde{\Delta}^2}{2}\right)\right)\left\{1 + \mathrm{erf}\left(\frac{t - (\mu + k\tilde{\Delta}^2)}{\sqrt{2}\tilde{\Delta}}\right)\right\}$$

Typically, with streak camera measurements the IRF can be well approximated by a sum of up to three Gaussians.

The solution of the general compartmental model described by the *K* matrix consists of exponential decays with decay rates equal to the eigenvalues of the *K* matrix. When the compartmental model consists of independently decaying species their spectra are termed $DAS_l(\lambda)$ (decay associated spectra), and when it consists of a sequential scheme with increasing lifetimes the spectra are termed $EAS_l(\lambda)$ (evolution associated spectra).

The interrelation between the DAS and SAS is expressed in the following matrix equation:

$$C^D(\theta,\mu,\Delta)DAS^T = C^S(\theta,\mu,\Delta)SAS^T$$

Here the matrix $C^D(\theta,\mu,\Delta)$ contains in its *l*-th column the decay $c_l^D(t,k,\mu,\Delta)$ and the matrix $C^S(\theta,\mu,\Delta)$ contains in its columns the populations $c_l^S(t)$ of the general compartmental model.

Simultaneous target analysis: To resolve the different species and to improve the precision of the estimated parameters, the set of N_{exp} experiments that describe the same sample (measured with different excitation wavelengths or on different time ranges) can be analyzed simultaneously. For each additional data set TRS_e one scaling parameter α_e and one time shift parameter μ_e must be added:

$$TRS_e = \alpha_e(C_e^S(\theta,\mu_e,\Delta)SAS^T$$

The different excitation wavelengths are taken into account *via* the absorptions of the species that result in $C_e^S(\theta,\mu_e,\Delta)$. Since the two different excitation wavelengths (400 nm for predominant Chl excitation; 590 nm for predominant PB excitation) result in different initial concentrations of the compartments, the different species can be better resolved through simultaneous target analysis.

Residual analysis: Following a successfully converged fit, the matrix of residuals is analyzed with the help of a singular value decomposition (SVD). Formally the residual matrix can be decomposed as

$$res(t,\lambda) = \sum_{l=1}^{m} u_l^{res}(t)s_l w_l^{res}(\lambda)$$

where u_l and w_l are the left and right singular vectors, s_l the sorted singular values, and *m* is the minimum of the number of rows and columns of the matrix. The singular vectors are orthogonal, and provide an optimal least squares approximation of the matrix. The SVD of the matrix of residuals is useful to diagnose shortcomings of the model used, or systematic errors in the data.

Results and discussion

Measurements at room temperature: The ΔPSI absorption spectrum (orange) depicted in Fig. 1S*A* (*supplement available online*) clearly displays a decreased Chl *a* Q_y absorption band at ≈680 nm that is largely attributed to PSI in WT cells (green in Fig. 1S*A*). Still a shoulder is visible in the ΔPSI absorption spectrum at ≈680 nm, attributable to PSII Chl *a*. Likewise the Soret bands decreased in ΔPSI.

Fig. 3 depicts the estimated DAS. The black DAS represents equilibration between the rod phycocyanins PC640 and PC650 in 6–8 ps. The red DAS represents equilibration between the rods and the APC660 pigments of the core cylinders. The blue DAS differs for the 400 and 590 nm excitation. In the latter it is conservative and can be interpreted as equilibration between the PB and PSII. The green DAS is positive everywhere and can be interpreted as trapping by the open PSII RC (the 680 nm peak). The magenta DAS is also positive everywhere and can be interpreted as trapping in the closed PSII RC. These observations can further be tested with the help of a target analysis. Assuming that PB is the same *in vivo* and *in vitro* (Tian *et al.* 2011, 2012), we adopt the functional compartmental model for the PB from van Stokkum *et al.* (2017).

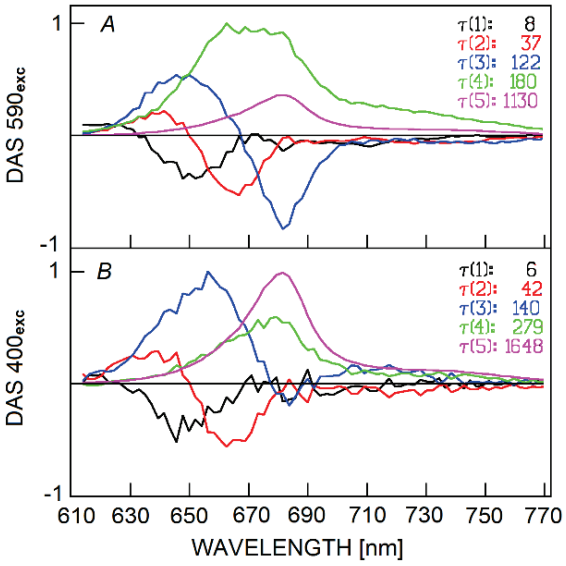

Fig. 3. Estimated DAS after 590 (*A*) or 400 (*B*) nm excitation at RT. The estimated lifetimes (in ps) are written in the legend at the right using the appropriate color.

Table 1. Estimated fractions of the different complexes in the experiments at RT in the four experiments (in acquisition order).

	590 exc	590 exc	400 exc	400 exc
	TR2	TR4	TR4	TR2
PB-PSII open	86%	84%	51%	49%
PB-PSII closed	8%	7%	24%	29%
non-transferring PB	6%	10%	25%	22%

It is based upon the schematic structure depicted in Fig. 2. The kinetic scheme contains six different types of functional compartments. Because the PB architecture possesses a C2 rotational symmetry axis, perpendicular to the membrane, the core can be described by three APC660 and one APC680 compartment (black). Three APC660 compartments are needed: the top cylinder (magenta), the APC660 pigments in the D and EF disks (orange), which are in the closest contact to the APC680 pigments,

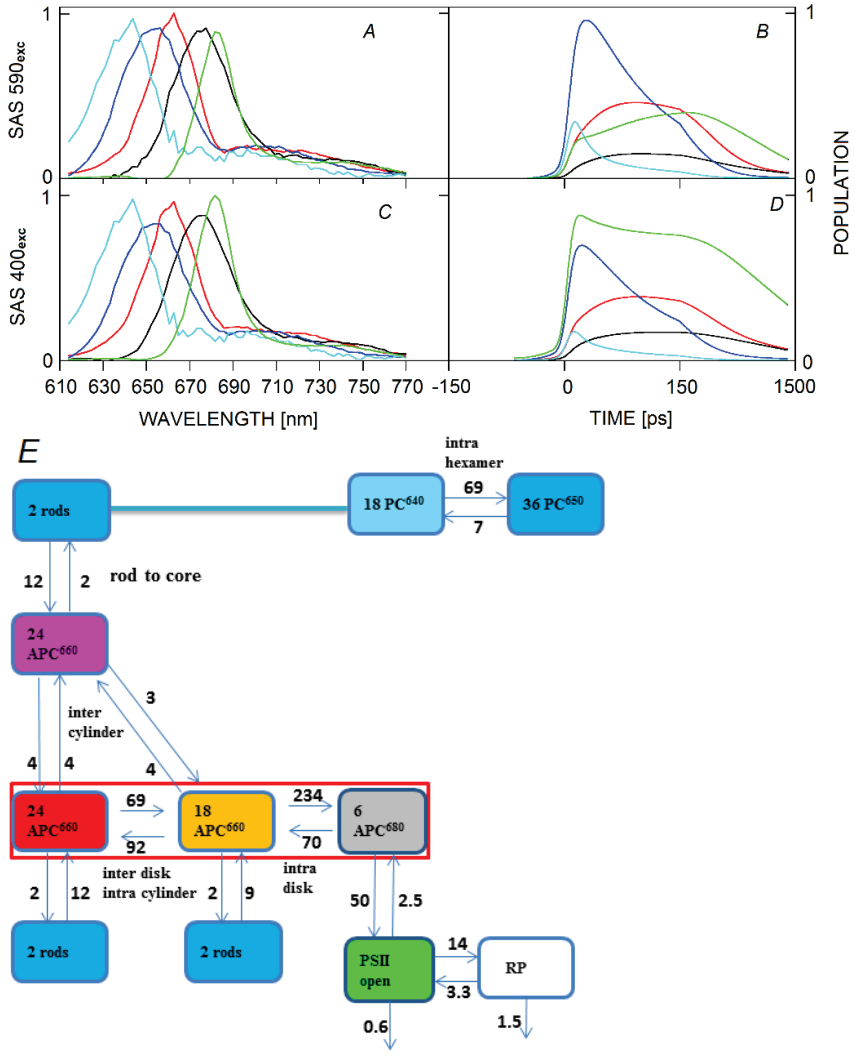

Fig. 4. Target analysis of the PB-PSII complex with RCs open at RT. Total concentrations and SAS estimated after 590 (*A,B*) or 400 (*C,D*) nm exc. Key: PC640 (cyan), PC650 (blue), APC660 (red), APC680 (black), and PSII Chl *a* (green). (*E*) Functional compartmental model, with a zoom out of a rod consisting of three lumped hexamers in the upper right. The magenta APC660 compartment represents the top cylinder. The red rectangle indicates the two basal cylinders. All microscopic rate constants are in 1/ns. The common k_{fl} rate constant for excited PC and APC states of 0.78/ns has been omitted for clarity.

Table 2. Percentage excitation of pigment type and between parentheses the relative absorption of a single pigment with the different excitation wavelengths at RT.

Excitation [nm]	PC640	PC650	APC660	APC680	PSII Chl *a*
590	37% (2)	37% (1)	11% (1)	1% (1)	14% (1.1)
400	14.5% (1)	29% (1)	9% (1)	1% (1)	46.5% (4.7)

Table 3. Amplitude matrix of the PB-PSII complex with RCs open at RT with 590 nm excitation. Color code of the species and estimated microscopic rates are given in Fig. 4*E*. Color code of the largest amplitudes indicates equilibration between compartments. Further explanation in the text.

Excitation	Species\lifetime [ps]	2.4	10.6	12.8	12.8	12.8	32	58	72	95	119	185	779
0.041	APC660	0	0	0.02	0	0	0.01	0	-0.30	-0.01	-0.04	0.35	0
0.041	APC660	-0.003	0.03	0	-0.02	0.01	-0.05	0	-0.07	0.05	0.03	0.06	0
0.031	APC660	0.012	-0.01	0	0.01	0	-0.03	0	-0.04	0.02	0.02	0.03	0
0.010	APC680	-0.010	-0.04	0	0.07	-0.01	-0.06	0	-0.10	0.05	0.04	0.06	0.01
0.123	PC650	0	0	-0.10	0	0	0	0	0.15	-0.02	-0.02	0.09	0
0.123	PC650	0	0	0	-0.10	0.01	0	0	0.04	0.13	0.02	0.02	0
0.123	PC650	0	0	0	-0.01	-0.08	0	0	0.01	-0.02	0.19	0.01	0
0.123	PC640	0	0	0.08	0	0	0	0	0.02	0	0	0.01	0
0.123	PC640	0	0	0	0.09	-0.01	0	0	0.01	0.02	0	0	0
0.123	PC640	0	0	0	0.01	0.07	0	0	0	0	0.02	0	0
0.140	PSII	0	0.03	0	-0.06	0.01	0.24	0.07	-0.66	0.17	0.11	0.04	0.20
0.000	RP	0	0	0	0.01	0	-0.13	-0.08	1.01	-0.41	-0.41	-0.79	0.79

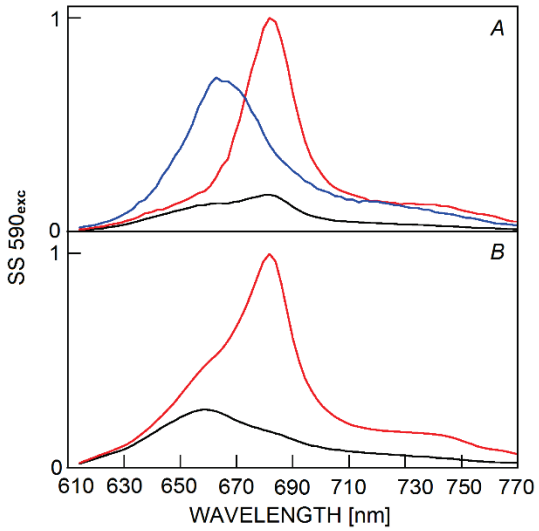

Fig. 5. (*A*) Reconstructed steady-state emission spectrum of the PB-PSII complex with open (*black*) or closed (*red*) RC and of the PB (blue). (*B*) steady-state emission spectrum of the PB-PSII complex with open (*black*) or closed (*red*) RC from a decomposition reported in Acuña *et al.* (2016a).

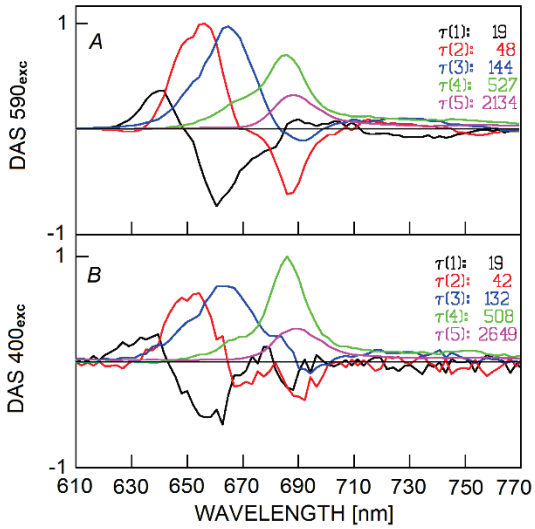

Fig. 6. Estimated DAS after 590 (*A*) or 400 (*B*) nm excitation at 77K. The estimated lifetimes [ps] are written in the legend at the right using the appropriate color.

and the remaining APC660 pigments of the basal cylinders (red). The red rectangle indicates the two basal cylinders. The intercylinder EET is described by an effective rate of 4/ns between the magenta and red APC660 compartments (van Stokkum *et al.* 2017). The microscopic rate constants connecting the compartments must obey detailed balance. In particular, the rate constants towards the orange APC660 compartment which contains 18 pigments, are 18/24 times as large as the analogous rate constants towards the red APC660 compartment which contains 24 pigments. The simplest description of a rod contains two types of functional compartments: PC640 (cyan) and PC650 (blue). It is assumed that two rods are connected to the top cylinder, whereas four rods radiate from the two basal cylinders. Again, the EET rates to the APC660 compartments from the rods obey detailed balance. Note that this is also an effective rate, which also takes into account the fast EET between the hexamers (van Stokkum *et al.* 2017). All PB rate constants were fixed to the values estimated in van Stokkum *et al.* (2017) that successfully described the PB EET. Our target model consists of three different complexes: a PB-PSII complex with RCs open (estimated to be 86% with 590 nm excitation and TR2) or closed (8%) and non-transferring PB (6%) (Table 1). In the experiments with 400 nm excitation the fraction PB-PSII complexes with RCs open was about twice as large as the fraction PB-PSII complexes with RCs closed (Table 1). The differences in the fractions between the two excitation wavelengths explain the differences between their fourth and fifth DAS (*cf.* Fig. 3).

The amount of loose PSII is assumed to be negligible, and in the modelling it cannot easily be distinguished from

PSII that is attached to PB. The kinetic schemes for the PB-PSII complex with RCs open or closed are depicted in Fig. 4*E* and Fig. 2S (*supplement available online*), respectively. In van Stokkum *et al.* (2017), the estimated relative precision of each rate constant was 20%. Here, we estimated that the rate of EET from the APC680 compartment to the PSII open compartment is (50 ± 10)/ns, whereas the backward rate was (2.5 ± 0.5)/ns. This ratio of the forward and backward rate constants is consistent with a small energy difference (677.5 *vs*. 681.7 nm) on top of a large entropy difference. A PSII dimer contains 2 × 39 = 78 chlorins. The energy difference between the APC680 and PSII maxima of 677.5 and 681.7 nm is 91/cm or 11 meV. The entropy difference between compartments with 78 and 6 pigments is $k_B T ln\left(\frac{N_1}{N_2}\right) = k_B T ln\left(\frac{78}{6}\right)$ which is 65 meV at room temperature. Thus the free energy of the green PSII compartment is assumed to be 76 meV lower than that of the grey APC680 compartment, which corresponds to a ratio of the backward to forward rate constants of 0.05. An effective EET rate to PSII of 10.4/ns has been reported in Maksimov *et al.* (2011). This rate can be interpreted as an overall effective EET rate from the PB to PSII. The estimates EET rates of Fig. 4*E* are consistent with calculations of Förster energy transfer rates in rods (Xie *et al.* 2002).

The estimated SAS depicted in Fig. 4*A*,*C* are consistent with the properties of the five types of pigments. The maxima of the emission are at 644, 656, 663, 677.5, and 681.7 nm for, respectively, PC640 (cyan), PC650 (blue), APC660 (red), APC680 (black), and PSII Chl *a* (green). The fit quality of the target analysis is good, *cf*. Figs. 3S, S, and 5S (*supplements available online*). Next to the kinetic scheme and its parameters also the relative absorption4s of the different pigments with the different excitation wavelengths have to be estimated. The time-zero spectrum is the weighted sum of the SAS of all the excited pigments. Thus, the shape of the SAS of the fastest decaying species, PC640, is the most sensitive to the relative absorption parameters. The parameters of Table 2, which led to the acceptable SAS of Fig. 4, were thus determined iteratively. Based upon this relative absorption the percentage excitation of each pigment type can be calculated. Both numbers are collated in Table 2 and are consistent with the properties of the five types of pigments. In panels *B* and *D* of Fig. 4, the total concentration is plotted. For each species, the total concentration is the sum of all excited state populations in the compartments with the spectrum of that species. Thus, the populations of the three APC660 compartments are summed, *etc*. Note that the initial population of PSII Chl *a* greatly increases with 400 nm excitation (Fig. 4*D*), which is absorbed well due to the Soret band of Chl *a*.

The amplitude matrix of the PB-PSII complex with open RC with 590 nm excitation is shown in Table 3. The fastest equilibration is between the orange APC660 and APC680 species, 2.4 ps (purple shading). Then with a 13 ps time constant the PC640 and PC650 pigments equilibrate (yellow shading). The first rod to core equilibration time constant is 72 ps (blue shading). The subsequent rod to core equilibration time constants are 95 and 119 ps. Intercylinder equilibration is visible as the decay of the magenta APC660 with a time constant of 185 ps. The energy transfer from APC680 to PSII is visible with time constants of 12.8 and 32 ps (green shading). In the PSII with open RC several time constants contribute to the charge separation, the fastest is 32 ps. The fully equilibrated PB-PSII complex with RCs open (which has 79% of the population residing in the RP state) ultimately decays with 779 ps. Note that the decay of the PSII Chl *a* emission is highly multiexponential due to the many EET time scales in the PB and to the equilibrium with the RP state.

After this successful target analysis we can now reconstruct the steady-state emission spectra (SS) of the three different complexes, cf. Fig. 5*A*. In the PB-PSII complex with RCs open the SS (black) has of course a much smaller area than the complex with RCs closed (red). Both SS have their maximum at 682 nm, whereas the maximum of the non-transferring PB SS is at 663 nm. In Fig. 5*B* we reproduced the steady state emission spectrum of the PB-PSII complex with open (black) or closed (red) RC from a decomposition of spectrally resolved fluorescence traces that were recorded over several minutes with 100 ms time resolution and were reported in Acuña *et al.* (2016a). We note that the relative areas of the complexes with RCs open or closed are consistent. The absence of a maximum at 682 nm in the black SS of Fig. 5*B* suggests that the decomposition reported in Acuña *et al.* (2016a) was suboptimal.

Measurements at 77K: Fig. 6 depicts the estimated DAS at 77K. The black DAS represents equilibration between the rod phycocyanins PC640 and PC650 in 19 ps and also the beginning of the equilibration between the rods and the APC660 pigments of the core cylinders. The red DAS represents the final equilibration between the rods and the core, and most probably also a rise of PSII Chl *a* near ≈685 nm. The blue DAS is nonconservative, representing a loss of emission with ≈140 ps, in combination with a small rise of PSII Chl *a* near ≈690 nm. The green DAS is positive everywhere and can be interpreted as quenching (that probably involves formation of a radical pair) in the closed PSII RC (the 680 nm peak) (Snellenburg *et al.* 2017), with an additional loss below 675 nm that can be attributed to non-transferring PB. The magenta DAS is also positive everywhere and can be interpreted as decay of the red shifted emission of the equilibrated closed PSII RC.

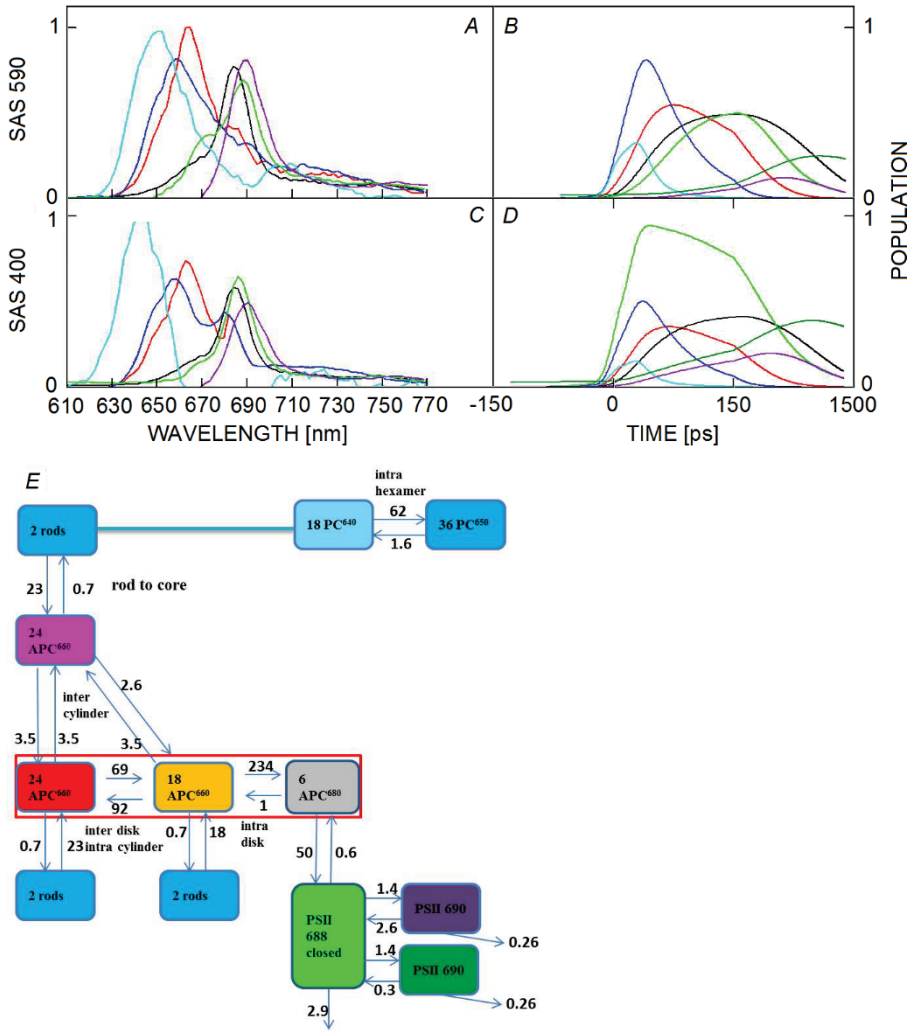

Fig. 7. Target analysis of the PB-PSII complex with RCs closed at 77K. Total concentrations and SAS estimated after 590 (*A,B*) or 400 (*C,D*) nm exc at 77K. Key: PC640 (cyan), PC650 (blue), APC660 (red), APC680 (black), PSII Chl *a* (green), and PSII 690 (dark green and purple, same SAS). (*E*) Functional compartmental model, with a zoom out of a rod consisting of three lumped hexamers in the upper right. All microscopic rate constants are in 1/ns. The common k_{fl} rate constant for excited PC and APC states of 1.4/ns has been omitted for clarity. Further explanation in the text.

Our target model consists of two different complexes: a PB-PSII complex with RCs closed (estimated to be 80% with 590 nm excitation and TR2) and non-transferring PB (20%) (Table 1S, *supplement available online*)).

Since no functional model of the PB at 77K is available, we start out from the PB model of Fig. 4*E*. Recently, a functional model of the PSII core at 77K has been established (Snellenburg *et al.* 2017). Three compartments were needed, one for the bulk Chl *a*, including the RC, from which excitations are quenched with a rate of ≈3/ns. Two more compartments describe the equilibration with red shifted Chl *a* in the core antennae CP43 and CP47. Since we have only limited data available, we assume equality of these two red shifted Chl *a* SAS. The functional model of the PB at 77K is depicted in Fig. 7*E*. Note that all uphill rate constants (from PC650 to PC640, from APC660 to PC650, from APC680 to APC660, and from PSII to APC680) had to be free parameters, since at 77K the thermal energy is four times smaller than at RT. In addition, we released three more rate constants, from PC640 to PC650, from PC650 to APC660, and the slow intercylinder equilibration rate. These were estimated to be different from the values estimated at RT (*cf.* Fig. 7*E*). The largest difference found was the rate from PC650 to APC660, which increased from 12 to 23/ns. This suggests that the structure at 77K more favors the rod to core energy transfer. Most importantly, also the 77K data are consistent with an energy transfer rate of 50/ns [= $(20\ \text{ps})^{-1}$] from APC680 to PSII. The fit quality of the target analysis is good, *cf.* Fig. 6S and Fig. 7S (*supplements available online*). The estimated SAS depicted in Fig. 7*A*,*C* are consistent with the properties of the six types of pigments. The maxima of the SAS are at 642, 656, 663, 684, 688, and 690 nm for, respectively, PC640 (cyan), PC650 (blue),

APC660 (red), APC680 (black), bulk and red PSII Chl *a* (green, purple). The SAS estimated with 590 nm exc (Fig. 7*A*) are attenuated on the blue side because a cut off filter had to be used to suppress the scattered excitation light. The PC650 and APC660 SAS (blue and red), estimated with 400 nm exc (Fig. 7*C*) show small humps in the 680 nm region. Thus more measurements at 77K are needed, in particular to resolve the differences between the APC680 pigments that were observed in mutants (Jallet *et al.* 2012, Acuña *et al.* 2016b).

Analogous to Table 2, the percentage excitation of each pigment type can be calculated, as well as the relative absorption per pigment. Both numbers are collated in Table S2 and are consistent with the properties of the five types of pigments. With 590 nm excitation light, two main differences between RT and 77K are: first, light is more selectively absorbed by PC640, which is to be expected because the line hapes are narrower at 77K, thus favoring the PC640 pigment that absorbs nearer to 590 nm. Second, less PSII Chl *a* absorption appears to be present at 77K.

Conclusion: From this study we can conclude that the APC680 pigments of the PB transfer their energy with a rate of 50/ns [= $(20\ ps)^{-1}$] to PSII (Fig. 4*E*). More research will be needed to figure out the roles of the different types of APC680 pigments (Fig. 2). The next challenge will be to establish the rate of energy transfer to PSI in the PB-PSII-PSI megacomplex that is present in WT *Synechocystis* (Liu *et al.* 2013, Acuña *et al.* 2016a).

References

Acuña A.M., Kaňa R., Gwizdala M. *et al.*: A method to decompose spectral changes in *Synechocystis* PCC 6803 during light-induced state transitions. – Photosynth. Res. **130**: 237-249, 2016a.

Acuña A.M., Snellenburg J.J., Gwizdala M. *et al.*: Resolving the contribution of the uncoupled phycobilisomes to cyanobacterial pulse-amplitude modulated (PAM) fluorometry signals. – Photosynth. Res. **127**: 91-102, 2016b.

Adir N.: Elucidation of the molecular structures of components of the phycobilisome: reconstructing a giant. – Photosynth. Res. **85**: 15-32, 2005.

Arteni A.A., Ajlani G., Boekema E.J.: Structural organisation of phycobilisomes from *Synechocystis* sp strain PCC6803 and their interaction with the membrane. – Biochim. Biophys. Acta **1787**: 272-279, 2009.

Gillbro T., Sandstrom A., Sundstrom V. *et al.*: Picosecond study of energy-transfer kinetics in phycobilisomes of *Synechococcus* 6301 and the mutant AN 112. – Biochim. Biophys. Acta **808**: 52-65, 1985.

Glazer A.N.: Phycobilisome - a macromolecular complex optimized for light energy-transfer. – Biochim. Biophys. Acta **768**: 29-51, 1984.

Govindjee, Shevela D., Björn L.O.: Evolution of the Z-scheme of photosynthesis: a perspective. – Photosynth. Res. **133**: 5-15, 2017.

Holzwarth A.R.: Data analysis of time-resolved measurements. – In: Amesz J., Hoff A.J. (ed.): Biophysical Techniques in Photosynthesis. Pp. 75-92. Kluwer, Dordrecht 1996.

Jallet D., Gwizdala M., Kirilovsky D.: ApcD, ApcF and ApcE are not required for the Orange Carotenoid Protein related phycobilisome fluorescence quenching in the cyanobacterium *Synechocystis* PCC 6803. – Biochim. Biophys. Acta **1817**: 1418-1427, 2012.

Liu H., Zhang H., Niedzwiedzki D.M. *et al.*: Phycobilisomes Supply excitations to both photosystems in a megacomplex in cyanobacteria. – Science **342**: 1104-1107, 2013.

Maksimov E.G., Kuzminov F.I., Konyuhov I.V. *et al.*: Photosystem 2 effective fluorescence cross-section of cyanobacterium *Synechocystis* sp. PCC6803 and its mutants. – J. Photoch. Photobio. B **104**: 285-291, 2011.

Mirkovic T., Ostroumov E.E., Anna J.M. *et al.*: Light absorption and energy transfer in the antenna complexes of photosynthetic organisms. – Chem. Rev. **117**: 249-293, 2017.

Sandström A., Gillbro T., Sundström V. *et al.*: Picosecond study of energy-transfer within 18-S particles of AN-112 (a mutant of *Synechococcus* 6301) phycobilisomes. – BBA-Bioenergetics **933**: 54-64, 1988.

Scott M., McCollum C., Vasil'ev S. *et al.*: Mechanism of the down regulation of photosynthesis by blue light in the cyanobacterium *Synechocystis* sp PCC 6803. – Biochemistry **45**: 8952-8958, 2006.

Shen G., Boussiba S., Vermaas W.F.: *Synechocystis* sp PCC 6803 strains lacking photosystem I and phycobilisome function. – Plant Cell **5**: 1853-1863, 1993.

Snellenburg J.J., Dekker J.P., van Grondelle R. *et al.*: Functional compartmental modeling of the photosystems in the thylakoid membrane at 77 K. – J. Phys. Chem. B **117**: 11363-11371, 2013.

Snellenburg J.J., Wlodarczyk L.M., Dekker J.P. *et al.*: A model for the 77 K excited state dynamics in *Chlamydomonas reinhardtii* in state 1 and state 2. – Biochim. Biophys. Acta **1858**: 64-72, 2017.

Tian L., Farooq S., van Amerongen H.: Probing the picosecond kinetics of the photosystem II core complex *in vivo*. – Phys. Chem. Chem. Phys. **15**: 3146-3154, 2013a.

Tian L., Gwizdala M., van Stokkum I.H.M. *et al.*: Picosecond kinetics of light harvesting and photoprotective quenching in wild-type and mutant phycobilisomes isolated from the cyanobacterium *Synechocystis* PCC 6803. – Biophys. J. **102**:1692-1700, 2012.

Tian L., van Stokkum I.H.M., Koehorst R.B.M. *et al.*: Site, rate, and mechanism of photoprotective quenching in cyanobacteria. – J. Am. Chem. Soc. **133**: 18304-18311, 2011.

Tian L., van Stokkum I.H.M., Koehorst R.B.M. *et al.*: Light harvesting and blue-green light induced non-photochemical quenching in two different c-phycocyanin mutants of *Synechocystis* PCC 6803. – J. Phys. Chem. B **117**: 11000-11006, 2013b.

van Grondelle R., Dekker J.P., Gillbro T. *et al.*: Energy transfer and trapping in photosynthesis. – BBA-Bioenergetics **1187**:

1-65, 1994.
van Stokkum I.H.M., Gwizdala M., Tian L. *et al.*: A functional compartmental model of the *Synechocystis* PCC 6803 phycobilisome. – DOI: 10.1007/s11120-017-0424-5, 2017.
van Stokkum I.H.M., Larsen D.S., van Grondelle R.: Global and target analysis of time-resolved spectra. – BBA-Bioenergetics **1657**: 82-104, 2004.
van Stokkum I.H.M., van Oort B., van Mourik F. *et al.*: (Sub)-Picosecond spectral evolution of fluorescence studied with a synchroscan streak-camera system and target analysis. – In: Aartsma T.J., Matysik J. (ed.): Biophysical Techniques in Photosynthesis. Pp. 223-240. Springer, Dordrecht 2008.
Watanabe M., Ikeuchi M.: Phycobilisome: architecture of a light-harvesting supercomplex. – Photosynth. Res. **116**: 265-276, 2013.
Wlodarczyk L.M., Dinc E., Croce R. *et al.*: Excitation energy transfer in *Chlamydomonas reinhardtii* deficient in the PSI core or the PSII core under conditions mimicking state transitions. – Biochim. Biophys. Acta **1857**: 625-633, 2016.
Xie J., Zhao J.-Q., Peng C.: Analysis of the disk-to-disk energy transfer processes in C-phycocyanin complexes by computer simulation technique. – Photosynthetica **40**: 251-257, 2002